Integrating numerical and experimental geodynamo models

Douglas H. Kelley, Santiago Andrés Triana, Daniel S. Zimmerman, Donald H. Martin, and Daniel P. Lathrop · Departments of Physics and Geology, IREAP, and IPST · University of Maryland

Abstract

The recent history of the geodynamo problem chronicles great successes, from self-generation in many numerical simulations to the recent Bullard-von Karman dynamo achieved in an experiment by Monchaux *et al.* (2007). These successes give rise to opportunity for new insights via collaboration between numerics and experiment, with experiment offering benchmarks to numerics and numerics offering predictive power to experiment. We are pursuing such collaborations, first in a project with B. A. Buffett and H. Matsui (funded by NSF-CSEDI), and also by inviting further collaboration. Our experimental apparatus is an Earth-like spherical Couette flow, 60 cm in diameter and containing 110 L of liquid sodium (see Kelley *et al.* 2007). The inner and outer containers, both spherical, rotate independently. Such a geometry has boundary conditions readily amenable to numerical simulation. Moreover, it displays magnetohydrodynamic behaviors that are intricate and complex, but have large-scale features likely to be reproducible numerically. Here we present results from a variety of experiments—some with a copper inner sphere, and some with a soft iron inner sphere. We measure the exterior magnetic field using an array of Hall proves and project onto Gauss coefficients up to degree four. We are making sets of Gauss coefficient time series publicly available:

`http://complex.umd.edu/interestingdata`.

This is done with the hope of stimulating comparisons (benchmarks) with multiple groups developing numerical models.

Meridional probe array

Experimental setup

Our experimental work in spherical Couette flow is directly motivated by the geometry of Earth's core; we seek to match as many of the governing parameters as possible. Following previous work (Shew, 2004) that explored rotating convection, this apparatus is designed to mimic the geometry of the core with two independently rotating concentric spheres, radii a=10 cm and b=30 cm, and 110 L of liquid sodium between them. A DC magnetic field $\mathbf{B}_0$ parallel to the rotation axis, with magnitude 150 G, is applied by a pair of external electromagnets. The bulk of our data comes from an array of 25 Hall probes, which measure the component of the magnetic field along a cylindrical radius (B_r) at 21 locations along a meridian and four additional locations around the equator. One more Hall probe measures the axial component of the field (B_z) near the lower pole (see diagram).

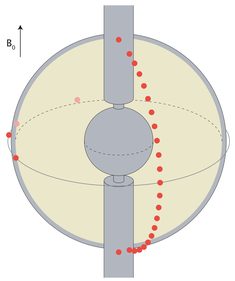

Observed Inertial Modes

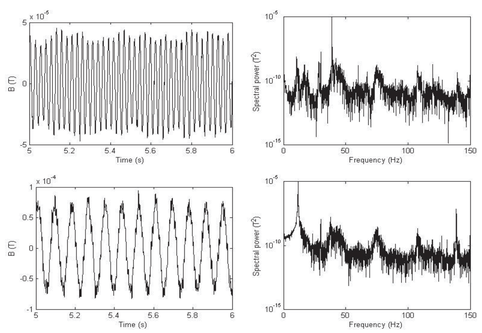

Two time series from a single Hall probe, showing measurements of induction in the presence of a constant, axial magnetic field, along with their power spectra. Experimental parameters are $(\Omega_i,\Omega_o)/2\pi$=(5.7,29.9) Hz, upper; $(\Omega_i,\Omega_o)/2\pi$=(-12.2,29.9) Hz, lower.

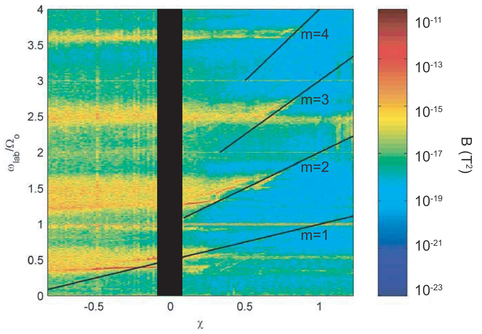

Spectrogram of inner sphere ramp showing oscillatory modes. Normalized rotation rate $\chi=\Omega_i/\Omega_o$ varies along the horizontal axis, and normalized signal frequency (from an equatorial Hall probe) ω_{lab}/Ω_o varies along the vertical. Color indicates power spectral density. Black lines show Mach 2 boundaries; see below. Here $\Omega_o/2\pi$=29.9 Hz.

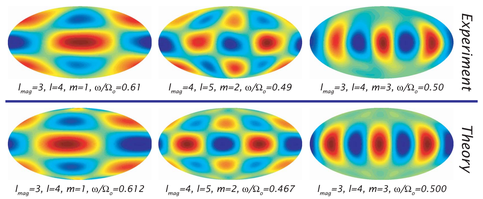

Induction B_r/B_0 at the surface, over one revolution of the dominant pattern, shown as a Mollweide projection: experimental data, first row; theoretical prediction, second row. Red indicates outward flux; blue, inward. The agreement in degree l, order (azimuthal wavenumber) m, frequency ω/Ω_o, and induction pattern between experimental data and theoretical predictions indicates the presence of inertial modes. Special thanks go to our co-author and collaborator Andreas Tilgner, who calculated the theoretical predictions.

Over-reflection

What mechanism forces these inertial modes? A shear layer between two fluid regions can reflect waves, and Ribner (1957) showed that if the Mach number between the two regions M>2, over-reflection can amplify the waves. In our experiment,

$$M = \frac{m\Omega_o}{\omega}(\chi - 1)$$

Setting M=2 and m=(1,2,3,4) yields the lines plotted on the spectrogram, above. As these lines bound the regions where inertial waves are present, we conclude that over-reflection is the likely forcing mechanism.

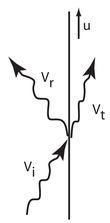

Open questions

Geometry: Our experimental data, taken in a spherical shell geometry, agrees well with theoretical wave modes for the full sphere. What role do the inner sphere and shaft play?

Mode selection: An infinite number of inertial modes are possible; we observe only a few. What mechanism selects them?

Symmetry: All modes we observe are anti-symmetric with respect to reflection across the equator, though the boundaries of our experiment are spherical. What breaks the symmetry?

Dynamo: Given their net helicity, might inertial modes like these, given sufficient strength, produce a dynamo? What role do inertial modes play in the geodynamo?

Gauss probe array

Experimental setup

Our more recent experiments employ an array of 30 Hall probes, positioned to allow for projection of the magnetic induction pattern onto the vector spherical harmonics up to degree four, yielding Gauss coefficients. We have also installed magnets that allow us to apply external fields up to 400 G. The resulting parameter space, in dimensionless quantities, is defined by the rotation rate ratio χ, magnetic Reynolds number Rm, and Lundquist number S. Accessible ranges are listed below. A variety of experimental results are shown below, some recorded with a copper inner sphere, and others recorded with a soft iron inner sphere of the same geometry. Material properties of the soft iron are given below as well.

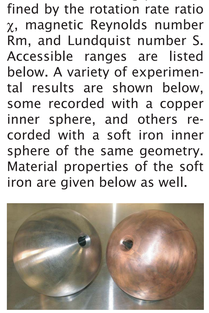

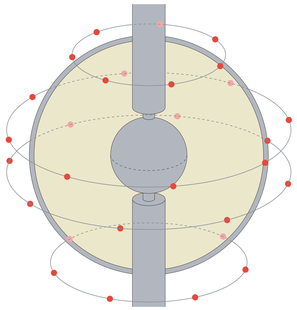

Dimensionless Parameters

Magnetic Prandtl number $Pm = \frac{\nu}{\eta} = 1.2 \times 10^{-6}$

Radius ratio $\frac{a}{b} = 0.33$

Rotation rate ratio $\chi = \frac{\Omega_i}{\Omega_o} \quad 0.15 \le |\chi| \le 180$

Lundquist number $S = \frac{B_0 b}{\eta\sqrt{\rho\mu_0}} \quad 0 \le S \le 4.2$

Magnetic Reynolds number $Rm = \frac{(\Omega_i - \Omega_o)b^2}{\eta}$

$-500 \le Rm \le 500$

Results: Copper sphere

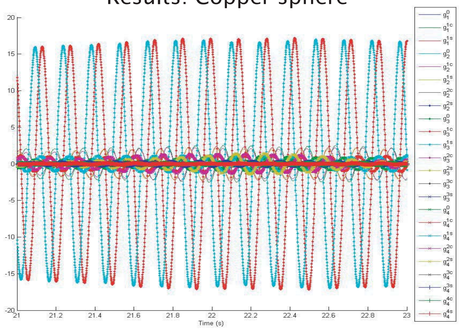

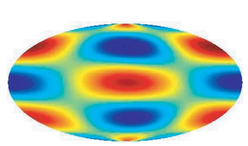

Above: *Time series of Gauss coefficients showing a propagating g_3^1 pattern. Parameters are $\Omega_i/2\pi$=3.2 Hz, $\Omega_o/2\pi$=18 Hz, B_0=124 G, or (χ,S,Rm) = (0.17,0.84,-105). **Left:** Snapshot of the magnetic induction on the surface of the sphere, with red indicating outward field and blue indicating inward field. This is the $(l_{mag},m,\omega/\Omega_o)$ = (3,1,0.612) inertial wave mode (see above).*

Soft Iron, ASTM A 848 Alloy 1

Typical composition: 99.634% Fe, 0.25% Mn, 0.04% Cu, 0.02% C, 0.02% Ni, 0.014% Si, 0.008% P, 0.007% S, 0.005% Ti, 0.002% Cr.

Maximum permeability	$5000\mu_0$	Hysteresis loss	250 J/m³/cycle at 10 kG
Minimum diffusivity	1.7×10^{-5} m²/s	Saturation	17.5 kG
Coercive force	64 A/m at 10 kG	Electrical resistivity	1.07×10^{-7} Ω m
		Linear expansion	1.36×10^{-5} 1/°C
		Melting point	1532 °C
		Curie temperature	760 °C
		Density	7860 kg/m³

Results: Soft iron sphere

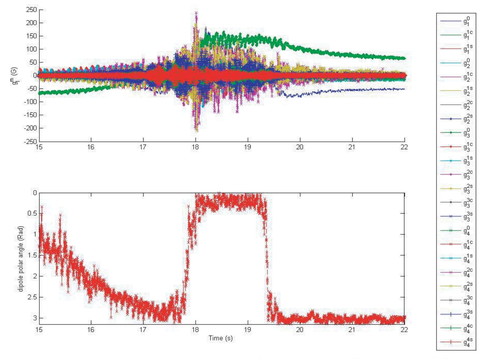

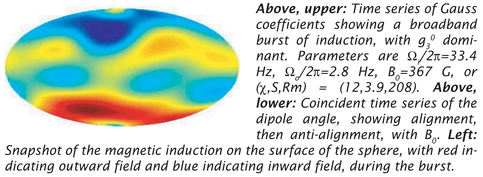

Above, upper: *Time series of Gauss coefficients showing a broadband burst of induction, with g_3^0 dominant. Parameters are $\Omega_i/2\pi$=33.4 Hz, $\Omega_o/2\pi$=2.8 Hz, B_0=367 G, or (χ,S,Rm) = (12,3.9,208). **Above, lower:** Coincident time series of the dipole angle, showing alignment, then anti-alignment, with B_z. **Left:** Snapshot of the magnetic induction on the surface of the sphere, with red indicating outward field and blue indicating inward field, during the burst.*

Below, upper: *Time series of Gauss coefficients showing reversal in g_3^0. Parameters are $\Omega_i/2\pi$=-38.9 Hz, $\Omega_o/2\pi$=4.6 Hz, B_0=210 G, or (χ,S,Rm) = (-8.5,2.2,-296). **Below, middle:** Coincident time series of motor torque. The shape suggests a Hopf bifurcation at the time of reversal of g_3^0. **Below, bottom:** Snapshots of the magnetic induction on the surface of the sphere, with red indicating outward field and blue indicating inward field, both before (**left**) and after (**right**) the reversal.*

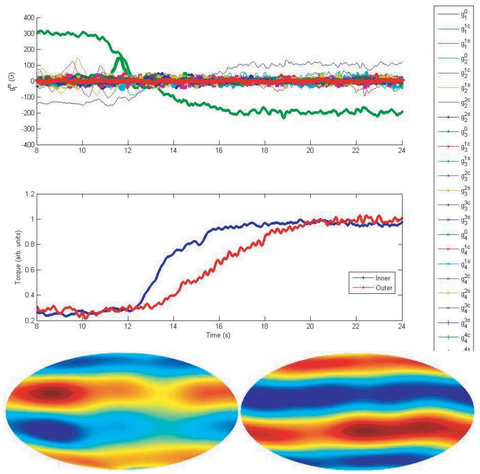

Three meter spherical Couette

Another experiment in progress, under construction for seven years, is our Three meter spherical Couette cell. It has identical geometry but is larger by a factor of five and is now operating with water as a test fluid.

Below, upper: *Time series of two pressure sensors, located away from the axis and near the top of the sphere, separated azimuthally by 90°. The correlation between the two signals likely indicates a propagating flow pattern with odd azimuthal wavenumber, m.* ***Below, bottom:*** *Spectrogram of pressure data recorded while increasing $\Omega_i/2\pi$ from 0 to 6 Hz with Ω_o=0. The dominant frequency increases linearly with Ω_i.*

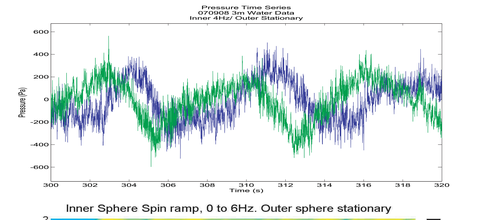

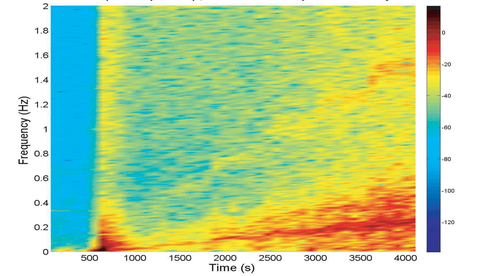

Integrating with numerical models

The container geometry, instrumentation, and data representation used in the experiments presented here have been chosen for ease of numerical modeling. While these experiments have realistic levels of turbulence, they also posses large-scale features possibly amenable to numerical models. Our hope is that we can benchmark numerical models via comparison with laboratory models, and make predictions about laboratory models via numerical models. Comments, suggestions, and collaborations are welcome!

References & Acknowledgements

Kelley, D. H. and Triana, S. A., and Zimmerman, D. S., and Tilgner, A., and Lathrop, D. P., Inertial waves driven by differential rotation in a planetary geometry. *Geophys. Astro. Fluid.*, **101**, 5/6, 2007.

Monchaux, R. and Berhanu, M. and Bourgoin, M. and Moulin, M. and Odier, Ph. and Pinton, J. -F. and Volk, R. and Fauve, S. and Mordant, N. and Petrelis, F. and Chiffaudel, A. and Daviaud, F. and Dubrulle, B. and Gasquet, C. and Marie, L. and Ravelet, F. Generation of a Magnetic Field by Dynamo Action in a Turbulent Flow of Liquid Sodium. *Phys. Rev. Lett.*, 2007, 98:044502, 1-4.

Ribner, H. S., Reflection, transmission, and amplification of sound by a moving medium. *J. Acoust. Soc. Am.*, 1957, **29**, 435-441.

Shew, W. L. and Lathrop, D. P., Liquid sodium model of geophysical core convection. *Phys. Earth Plan. Int.*, 2005, **153**, 136-149.

This work is generously supported by the National Science Foundation through the following grants: NSF/CSEDI EAR-0652882, NSF/Geophysics EAR-0207789, NSF/MRI EAR-0116129.

Public data: http://complex.umd.edu/interestingdata

More information: http://complex.umd.edu · dhk@umd.edu